

# Journal of Materials Chemistry A

Accepted Manuscript



This is an *Accepted Manuscript*, which has been through the Royal Society of Chemistry peer review process and has been accepted for publication.

*Accepted Manuscripts* are published online shortly after acceptance, before technical editing, formatting and proof reading. Using this free service, authors can make their results available to the community, in citable form, before we publish the edited article. We will replace this *Accepted Manuscript* with the edited and formatted *Advance Article* as soon as it is available.

You can find more information about *Accepted Manuscripts* in the [Information for Authors](#).

Please note that technical editing may introduce minor changes to the text and/or graphics, which may alter content. The journal's standard [Terms & Conditions](#) and the [Ethical guidelines](#) still apply. In no event shall the Royal Society of Chemistry be held responsible for any errors or omissions in this *Accepted Manuscript* or any consequences arising from the use of any information it contains.

Cite this: DOI: 10.1039/c0xx00000x

www.rsc.org/xxxxxx

ARTICLE TYPE

# Exceptional Electrochemical Performance of Porous TiO<sub>2</sub>-Carbon Nanofibers for a Lithium Ion Battery Anode

Xiaoyan Li,<sup>a</sup> Yuming Chen,<sup>a</sup> Limin Zhou,<sup>\* a</sup> Yiu-Wing Mai<sup>ab</sup> and Haitao Huang<sup>c</sup>

Received (in XXX, XXX) Xth XXXXXXXXX 20XX, Accepted Xth XXXXXXXXX 20XX

DOI: 10.1039/b000000x

We have developed one-dimensional (1D) porous TiO<sub>2</sub>-carbon nanofibers (ODPTCNs) by a simple coaxial electrospinning technique combined with subsequent calcination treatment as anode materials for Li-ion batteries. The prepared ODPTCNs contain plentiful surface pores through which lithium ions can transport from outer space into inner space as storage regions, thus activating all the materials. In addition, the high conductivity of the overall electrode and porous structure aid Li<sup>+</sup> access and the rapid transportation of lithium ions, thus reducing the diffusion paths for Li<sup>+</sup> and yielding a better rate capability. The novel ODPTCNs show a remarkable specific reversible capacity of ~806 mAh g<sup>-1</sup> and a high volumetric capacity of ~1.2 Ah cm<sup>-3</sup>, and maintain the capacity of ~680 mA h g<sup>-1</sup> after 250 cycles at a current density of 100 mA g<sup>-1</sup> and exhibit an exceptional discharge rate capability of 5 A g<sup>-1</sup> while retaining a capacity of ~260 mAh g<sup>-1</sup> after 1600 cycles. The ODPTCNs will serve as excellent anode materials for next-generation, high-power, and environmentally benign Li-ion batteries.

## Introduction

Rechargeable lithium-ion batteries (LIBs) have attracted considerable attention due to their huge success in electronic devices such as electric vehicles (EV) and hybrid electric vehicles (HEV).<sup>1</sup> Notwithstanding these achievements, it is still a significant challenge to develop new high-performance electrode materials with a high energy density, excellent cyclability, and a high level of safety to meet the demanding requirements of high-power EVs and HEVs.<sup>2,3</sup> Titanium dioxide (TiO<sub>2</sub>) has emerged as a promising anode material for LIBs due to its low cost, environmental friendliness, and structural stability during lithium insertion/deinsertion. Most importantly, TiO<sub>2</sub> has a high working potential of over 1.5 V *versus* Li<sup>+</sup>/Li, which avoids the decomposition of the organic electrolyte and short circuits due to the formation of dendritic lithium.<sup>4-8</sup> However, the practical use of TiO<sub>2</sub> in LIBs has been frustrated by its low theoretical capacity (335 mAh g<sup>-1</sup>), poor electron transport, and inherently weak electronic conductivity.<sup>9-12</sup> Various strategies have been developed to circumvent the drawbacks of TiO<sub>2</sub>, such as i) designing one-dimensional (1D) nanostructured TiO<sub>2</sub> to enhance vectorial ion and electron transport; ii) interconnecting TiO<sub>2</sub> with carbonaceous materials or metal to improve the conductivity; iii) blending TiO<sub>2</sub> with active materials to increase the capacity; and iv) introducing a porous structure into the TiO<sub>2</sub> matrix to obtain a large lithium flux and shorten the lithium diffusion length, which results in the enhancement of the kinetics associated with lithium.<sup>13-15</sup> Although considerable progress has been made in anode structure and composition, a novel TiO<sub>2</sub> with a good combination of these characteristics is urgently required.

In this paper, we design and fabricate 1D porous TiO<sub>2</sub>-carbon nanofibers (ODPTCNs) with a large surface area and a highly porous structure by a straightforward, versatile coaxial

electrospinning technique with subsequent calcination. As anodes, the novel ODPTCNs fabricated by this way show a remarkable specific reversible capacity of ~806 mAh g<sup>-1</sup> and a high volumetric capacity of ~1.2 Ah cm<sup>-3</sup>, maintain the capacity of ~680 mA h g<sup>-1</sup> after 300 cycles at a current density of 100 mA g<sup>-1</sup>, and exhibit an outstanding discharge rate capability of 5 A g<sup>-1</sup> while retaining a capacity of ~260 mAh g<sup>-1</sup> after 1600 cycles.

## Experimental details

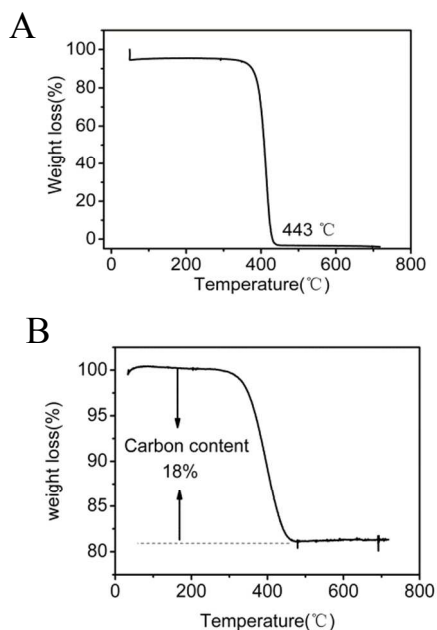
### Materials

Poly (methyl methacrylate) (PMMA) was purchased from Tokyo Chemical Industry Co., Ltd. Polystyrene (PS, M<sub>w</sub> ~280 000, Aldrich), tetraisopropyl titanate (Ti(OiPr)<sub>4</sub>, Aldrich) and dimethylformamide (DMF) were purchased from Aldrich.

### Synthesis of ODPTCNs

A typical coaxial electrospinning method was adopted in this work. The inner fluid of PMMA solution was fabricated by dissolving 1.5 g of PMMA in 30 mL of DMF solvent. For the outer solution, 3 g of PS was dissolved in 20 mL of DMF. Then 5 mL of Ti(OiPr)<sub>4</sub> and 4 mL of acetic acid were mixed into 20 mL of the PS solution to form the outer solution. In brief, the spinneret consisted of coaxial stainless-steel tubes. The distance between the cathode and the anode was kept at 20 cm and a high voltage of 17 kV was applied to the syringe needle tip and the metal collector by a power supply. Typical feeding rates for the coaxial solutions were set at 0.04 mm/min (KATO Tech Co., Ltd).

All of the experiments were conducted at room temperature in air. The resultant nanofibers were calcinated at 450 °C in Ar for 3 h to obtain the ODPTCNs.



5 **Fig.1** TGA analysis of (A) PS in Ar and (B) ODPTCNs in flowing air.

### Characterization

The morphology of the ODPTCNs was examined with a JEOL 10 6300F field-emission scanning electron microscopy (FESEM, JEOL, Japan) operated at 5 kV. High-resolution transmission electron microscopy (HRTEM), TEM-BF and secondary electron imaging in TEM (TEM-SEI) were performed using a JEOL 2100F transmission electron microscopy (JEOL, Japan) operated 15 at 200 kV with an electron energy loss spectroscopy (EELS) spectrometer (Gatan, Enfina). X-ray diffraction (XRD) patterns were collected on a Philips X'Pert Pro MPD X-ray diffractometer with Cu K  $\alpha$  radiation between 5° and 90°. The thermogravimetric analysis (TGA) was conducted under 20 atmospheric and Ar conditions using a Netzsch STA 449C thermogravimetric analyzer from room temperature to 700 °C at a heating rate of 10 °C min<sup>-1</sup>. The XPS spectra were measured on a Perkin-Elmer model PHI 5600 XPS system from a monochromated aluminum anode X-ray source. Ramam 25 spectroscopy was carried out with a Jobin-Yvon T6400 micro-Ramam system and an Ar<sup>+</sup> laser. Nitrogen adsorption-desorption isotherms at 77 k were performed by a Micromeritics, ASAP2020 analyzer. The pore-size distribution was calculated based on a non-local density functional theory method.

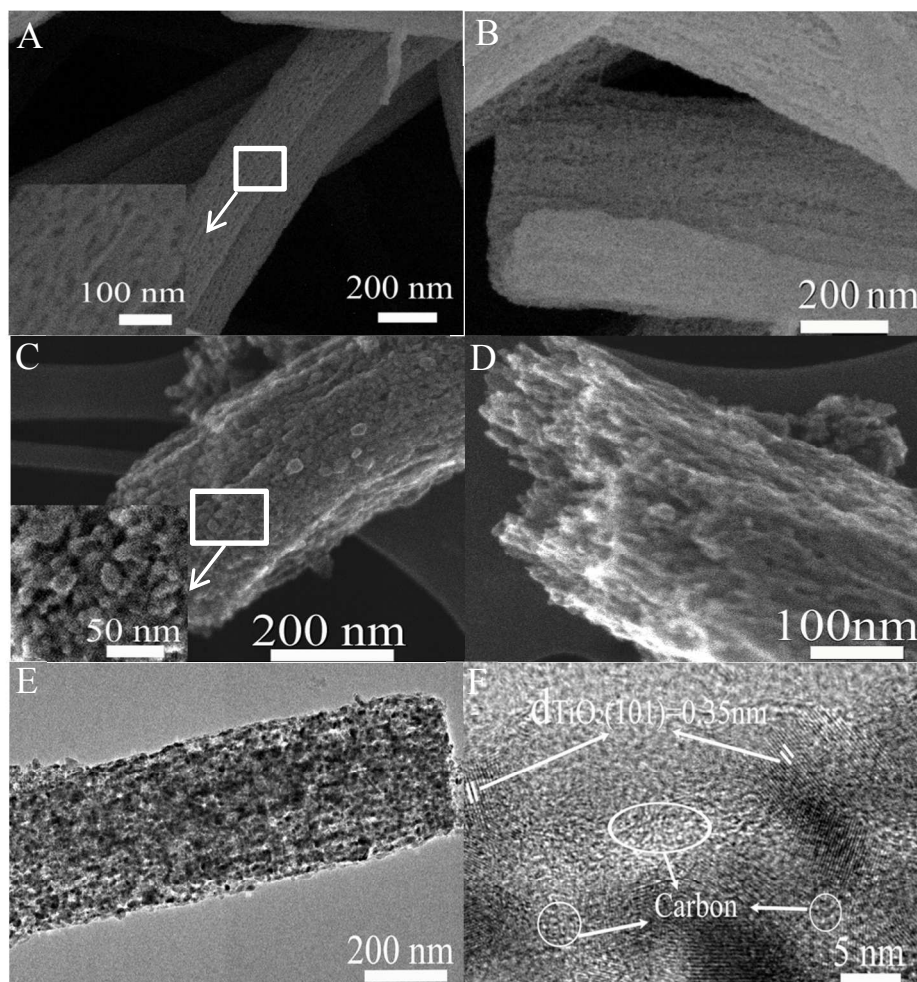


**Fig. 2** (A,B) FESEM, (C,D) TEM-SEI, (E) TEM, and (F) HRTEM images of the ODPTCNs.

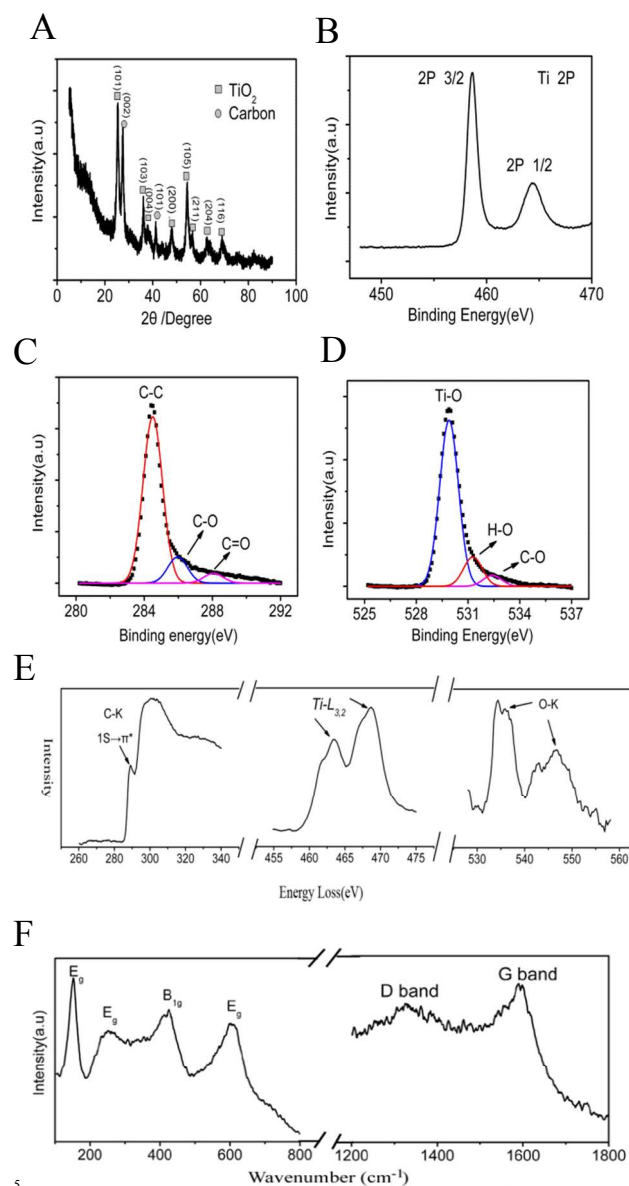


**Fig. 3** (A) X-ray diffraction patterns of the ODPTCNs. (B) Ti 2p, (C) C1s, and (D) O 1s high-resolution XPS spectrum. (E) EELS of C-K, Ti-L<sub>2,3</sub>, and O-K edges taken across the ODPTCNs interfaces. (F) Raman spectrum of the ODPTCNs.

### 10 Electrochemical characterization

The working electrode for the electrochemical measurements had a two-electrode coin-cell (CR 2032) configuration. A copper foil current collector pasted uniformly with a slurry of the ODPTCNs (80 wt.%), carbon black (10 wt.%) and poly(vinyl difluoride) (10 wt.%, PVDF) was dehydrated in a vacuum oven at 120 °C for 12 h. Cell assembly was carried out in a recirculating Ar glove box using the coated copper disk as the working electrode, metallic lithium as counter/reference electrode, celgard 2400 film as a separator film, and 1M LiPF<sub>6</sub> in ethylene carbonate (EC)/diethyl carbonate (DEC) (1:1 v/v) mixture as the electrolyte solution. The cells were discharged (Li<sup>+</sup> insertion) and charged (Li<sup>+</sup> de-

insertion) at different current densities in the 0-3 V voltage range on a LAND 2001 CT battery tester. Cyclic voltammetric (CV) was performed on a CHI 660C electrochemical workstation at a scan rate of 0.1 mV s<sup>-1</sup>.

### Results and Discussion

Two viscous liquids were simultaneously fed through the inner PMMA solution and the outer mixture of PS and Ti(OiPr)<sub>4</sub>, where PMMA served as the sacrificial component to produce pores, Ti(OiPr)<sub>4</sub> was the precursor of TiO<sub>2</sub>, and PS was the carbon source. During the electrospinning process, the PS and PMMA were mixed together because they had the same DMF solvent. The PMMA was distributed in the PS matrix and PS/Ti(OiPr)<sub>4</sub>/PMMA composite nanofibers were produced.<sup>2</sup> The resultant nanofibers were calcinated at 450 °C in Ar for 3 h to obtain the ODPTCNs. PS was selected as the carbon source for two main reasons. First, PS is a synthetic aromatic polymer that includes a benzene ring, which is a source of graphitic carbon. Second, PS can be completely decomposed at 450 °C in Ar (Fig. 1A). Here, the complete decomposition of PS was delayed by Ti<sup>4+</sup> interacting with the unsaturated bonds as a radical trapper to stabilize the unstabilized part, yielding 18 % carbonaceous materials and a porous structure in the ODPTCNs (Fig. 1B).<sup>16,17</sup>

The FESEM images in Fig. 2A and Fig.S1 indicates that 1D fibrous structure with a fiber diameter of ~400 nm is continuous over long distances, providing electrical and mechanical interconnections throughout the continuous network of nanofibers.<sup>18</sup> The highly porous surface of the ODPTCNs is shown in the inset of Fig. 2A, which accords with the TEM-SEI image (Fig. 2C). The porous structure is also observed on the fracture surface of the broken nanofibers, as shown in Fig. 2B, which is also similar to the TEM-SEI image in Fig. 2D. The pores create a large surface area, which is very important for LIB anode materials. Figure 2E shows the TEM image of an individual TiO<sub>2</sub>-carbon nanofiber and its corresponding HRTEM image is in Fig. 2F. It clearly shows TiO<sub>2</sub> nanocrystallines with diameter of ~15 nm incorporated with the carbon materials, as indicated by the arrows. The resolved inter-planar distance is ~ 0.35 nm, corresponding to the (101) plane of anatase TiO<sub>2</sub>.

The X-ray diffraction (XRD) pattern of the ODPTCNs in Fig. 3A shows two peaks at about 25.5° and 41.3°, which can be assigned to the (002) and (101) diffractions of the carbon. Others distinct diffraction peaks can be indexed to anatase TiO<sub>2</sub> (JCPDS 21-1272). Ti 2p XPS (X-ray photoelectron spectroscopy) spectrum in Fig. 3B shows the binding energies of 458.7 eV and 464.5 eV that correspond to the Ti 2p<sub>3/2</sub> and Ti 2p<sub>1/2</sub> respectively, and accord with the typical values of TiO<sub>2</sub>.<sup>19</sup> Figure 3C displays the C1s spectrum of the ODPTCNs. The C1s peak can be well split into three peaks located at ~284.5 eV, 285.9 eV, and 288.1 eV, representing the C-C, C-O, and C=O bonds, respectively.<sup>20</sup> The O1s spectrum can be fitted to three peaks (Fig. 3D): the peaks located at about 529.8 eV and 531.2 eV can be assigned to the oxygen from the TiO<sub>2</sub> crystal lattice and chemisorbed water, the other at ~532.3 eV is attributed to C-O-Ti bonding.<sup>21</sup>

The electron energy loss spectrum (Figure 3E) of the ODPTCNs indicates the presence of C-K, Ti-L<sub>3</sub>/L<sub>2</sub>, and O-K. An intense pre-peak of the carbon-K edge located at ~ 285 eV can be attributed to transition to π\* states in the sp<sup>2</sup>-bonded carbon,

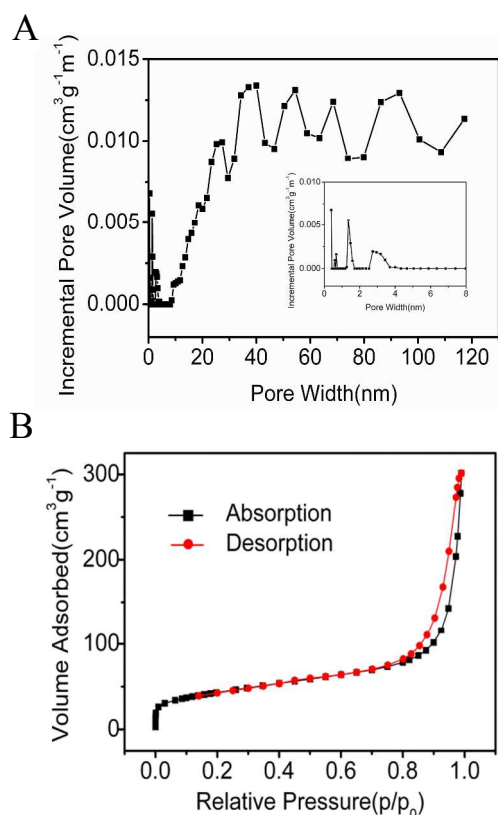


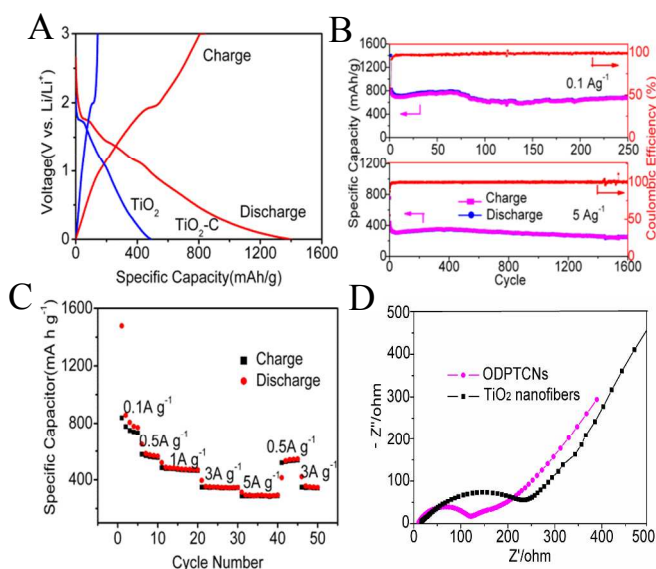
**Fig. 4** (A) Pore size distribution and (B) nitrogen adsorption-desorption isotherms of the ODPTCNs.

indicating the presence of graphitic carbon in the ODPTCNs.<sup>22</sup> A  $Ti-L_{3/2}$  edge located at approximately 463 and 468 eV is also observed in the ODPTCNs, which can be due to the electronic transitions from  $Ti\ 2p^63d^n$  to  $Ti\ 2p^53d^{n+1}$ . The non-splitting  $Ti-L_{3/2}$  edge suggests the octahedral coordination of titanium atoms with oxygen.<sup>23-25</sup> The O-K edge shows a single peak, confirming the unoccupied oxygen p state.<sup>26</sup> The Raman spectrum analyses also confirm the presence of anatase  $TiO_2$  and some graphitic carbon in the obtained materials (Fig. 3F). These results demonstrate that the ODPTCNs consist of anatase  $TiO_2$ , graphitic carbon, and amorphous carbon, which is consistent with the TEM and HRTEM observations.

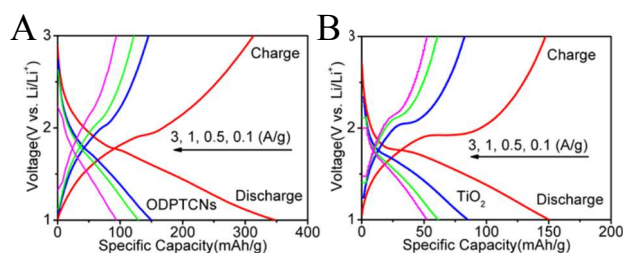
The surface and pore-size characterization of the ODPTCNs was performed by nitrogen adsorption-desorption experiments. The Brunauer-Emmett-Teller (BET) specific surface area of the ODPTCNs is  $\sim 153.1\ m^2\ g^{-1}$  with a total pore volume of  $0.47\ m^3\ g^{-1}$ . Figure 4A shows the results of a pore size analysis conducted by applying a hybrid nonlocal density functional theory. It is clear that the ODPTCNs possess micropores that peak at  $\sim 0.4$ , 0.7, and 1.3 nm, mesopores that peak at  $\sim 2.7$ , 25, 40, and 54 nm, and macropores that peak at  $\sim 68$ , 86, 93, and 117 nm. These results are also shown in the FESEM and TEM images. Additionally, the isotherms in Figure 4B are indexed to the typical type IV, which is associated with porous materials according to the classification of Langmuir.<sup>27,28</sup>

Figure 5A shows the galvanostatic voltage profiles of the ODPTCNs at a current density of  $100\ mA\ g^{-1}$  in the voltage range of 0-3 V versus  $Li^+/Li$ . For comparison, an electrode made of pure  $TiO_2$  nanofibers was also tested under the same

electrochemical conditions. It is noted that the first charge capacity for the ODPTCNs is  $\sim 806\ mAh\ g^{-1}$ , which is significantly higher than that of  $TiO_2$  nanofibers ( $142\ mAh\ g^{-1}$ ), the theoretical capacity of  $TiO_2$  ( $335\ mAh\ g^{-1}$ ), some metal oxides and other carbon materials including graphite ( $372\ mAh\ g^{-1}$ ), carbon nanotubes (CNT,  $210\ mAh\ g^{-1}$ ), carbon nanofibers (CNF,  $200\ mAh\ g^{-1}$ ), CNF/CNT ( $546\ mAh\ g^{-1}$ ) and graphene ( $453\ mAh\ g^{-1}$ ).<sup>2</sup> The volumetric capacity of the synthesized ODPTCNs electrode can be as high as  $\sim 1.2\ Ah\ cm^{-3}$ , which is approximately 1.4 times than that of graphite ( $0.837\ Ah\ cm^{-3}$ ).<sup>29</sup> The large irreversible capacity of  $606\ mAh\ g^{-1}$  is due to the formation of a solid electrolyte interface (SEI) layer on the surface of the ODPTCNs.<sup>2,29</sup> Fig.S2† shows the cyclic voltammograms (CV) of the DPTCN electrode at a scan rate of  $0.1\ mV\ s^{-1}$ . There are two obvious reduction peaks in the potential range of 0.4-0.7 V and 1-1.5 V in the first cycle, corresponding to irreversible reactions between the carbonaceous material and the electrolyte, the co-insertion of the lithium ion into carbon and the formation of SEI film.<sup>29,30</sup> A pair of pronounced anodic/cathodic peaks appear at 1.68 and 2.05 V, which can be ascribed to the Li-ion extraction/insertion in the anatase  $TiO_2$  lattice ( $TiO_2 + xLi^+ + xe^- \rightarrow Li_xTiO_2$ ).<sup>1,31</sup> Notably, the third CV curve onwards remains stable, indicating that the electrode is stable during the discharge-charge cycle following the first cycle. Figure 5B shows that the ODPTCNs exhibit excellent cyclic stability and retain a reversible capacity of  $\sim 680\ mAh\ g^{-1}$  after 250 cycles at a rate of  $100\ mA\ g^{-1}$  and  $260\ mAh\ g^{-1}$  after 1600 cycles at a rate of  $5\ A\ g^{-1}$ , whereas  $TiO_2$  nanofibers maintain only  $65\ mAh\ g^{-1}$  at a rate of  $100\ mA\ g^{-1}$  (Fig. S3†). And the coulombic efficiencies at both rates are more than 98 % after the first few cycles. Figure 5C shows the rate performance of the DPTCN electrode. At current densities of 0.1, 0.5, 1, 3 and  $5\ A\ g^{-1}$ , the reversible capacity of the ODPTCNs is about 800, 570, 480, 350 and  $300\ mAh\ g^{-1}$ , which are all higher than those of  $TiO_2$ -based nanomaterials as well as some metal oxides, carbonaceous



**Fig. 5** Electrochemical properties of the ODPTCNs as anode electrodes for Li-ion batteries. (A) Charge-discharge profiles of the ODPTCNs and  $TiO_2$  nanofibers at a current density of  $100\ mA\ g^{-1}$  between 3 and 0 V versus  $Li^+/Li$ . (B) Cycling performance of the ODPTCNs at different current densities between 3 and 0 V versus  $Li^+/Li$ . (C) Rate capability of the ODPTCNs. (D) Nyquist plots of the ODPTCNs and  $TiO_2$  electrodes with an amplitude of 5 mV in the frequency range from 100 kHz to 10 mHz.



**Fig. 6** Charge-discharge curves of the ODPTCNs (A) and TiO<sub>2</sub> nanofibers (B) electrodes obtained at different current densities in the voltage range of 1-3V.

materials and hybrid materials such as SnO<sub>2</sub>, CNFs, CNTs and MnO<sub>2</sub>-CNT.<sup>2,29,32-37</sup> Additionally, the prepared composites still have high capacities of ~313, 146, 121, and 94 mAh g<sup>-1</sup> at current densities of 0.1, 0.5, 1, and 3 A g<sup>-1</sup>, respectively, tested between 3 and 1 V versus Li<sup>+</sup>/Li, which is much higher than that of TiO<sub>2</sub> nanofibers (Fig.6). The electrode voltage decreases when the current density increases, 2.6 V at 1 A g<sup>-1</sup> and 2.2 at 3 A g<sup>-1</sup>, which is due to the sluggish diffusion kinetics of Li ions at high rate.<sup>38,39</sup> To further show the enhanced performance of the prepared materials, the comparisons of the capacities of the electrodes prepared by different TiO<sub>2</sub>-based materials are given in Table S1.<sup>40-44</sup> These results show that the ODPTCNs have a high reversible capacity, a good cycling stability and outstanding rate capability. Electrochemical impedance spectroscopy (EIS) measurements also show that the value of high-frequency semicircle in the ODPTCNs is much smaller than that of TiO<sub>2</sub> nanofibers, suggesting that the ODPTCNs electrodes possess a higher electrical conductivity and a more rapid charge-transfer reaction for lithium ion insertion and extraction (Fig. 5D).

The foregoing results show the prepared ODPTCNs to be an exceptional anode material for high-performance LIBs. There are several reasons for the superior electrochemical performance of the ODPTCNs. First, as shown in Fig. 7, the continuous network of 1D nanofibers serves as a channel for electron transportation, and the plentiful nanopores in the ODPTCNs act as reservoirs for the storage of Li<sup>+</sup> ions.<sup>2,3,45</sup> Second, the large surface area of the ODPTCNs provides a sufficient large electrode/electrolyte interface, which promotes the charge-transfer reactions.<sup>29</sup> Third, the nanoscale fibers, the porous structure, and the high conductivity of the overall electrode facilitate Li<sup>+</sup> access and the fast transportation of lithium ions, thus reducing the diffusion paths for Li<sup>+</sup> and yielding a better rate capability.<sup>8,37,45</sup> Finally, the 1D architecture maintains excellent mechanical integrity of the overall electrode during the lithiation/delithiation process.

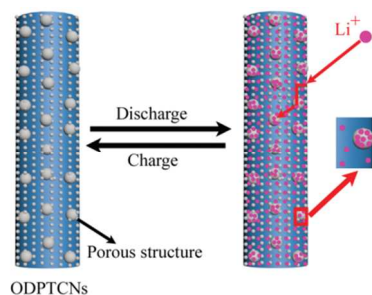


**Fig. 7** Schematic diagram illustrating the Li<sup>+</sup> insertion and deinsertion processes inside the ODPTCNs.

## Conclusions

In summary, we have prepared novel 1D porous TiO<sub>2</sub>-carbon nanofibers (ODPTCNs) by a simple coaxial electrospinning technique with subsequent treatment as anode materials for Li-ion batteries. The novel structure of the ODPTCNs resulted in remarkable electrochemical performance in the form of a high specific reversible capacity and an exceptional volumetric capacity, long cycling stability, and outstanding rate capability. The prepared ODPTCNs should prove to excellent anode materials for next-generation and high-power LIBs.

## Acknowledgements

The authors are grateful for the support received from the Research Grants Council of the Hong Kong Special Administration Region (grants: PolyU5349/10E; PolyU5312/12E) and the Hong Kong Polytechnic University (grant: 1-BD08).

## Notes and references

- <sup>a</sup> Department of Mechanical Engineering, The Hong Kong Polytechnic University, Hong Kong, China. Tel: 852-2766 6663; Fax: 852-2365 4703 E-mail: mmlmzhou@polyu.edu.hk
- <sup>b</sup> Centre for Advanced Materials Technology (CAMT), School of Aerospace, Mechanical and Mechatronics Engineering J07, The University of Sydney, NSW 2006, Australia.
- <sup>c</sup> Department of Applied Physics and Materials Research Center, The Hong Kong Polytechnic University, Hong Kong, China.
- L. Yu, Z. Y. Wang, L. Zhang, H. B. Wu and X. W. Lou, *J. Mater. Chem. A*, 2013, **1**,122.
- Y. M. Chen, Z. G. Lu, L. M. Zhou, Y. W. Mai and H. T. Huang, *Energy Environ. Sci.*, 2012, **5**, 7898.
- L. Qie, W. M. Chen, Z. H. Wang, Q. G. Shao, X. Li, L. X. Yuan, X. L. Hu, W. X. Zhang and Y. H. Huang, *Adv. Mater.* 2012, **24**, 2047.
- Y. C. Qiu, K. Y. Yan, S. H. Yang, L. M. Jin, H. Deng and W. S. Li, *ACS Nano*, 2010, **4**, 6515.
- G. N. Zhu, Y. G. Wang and Y. Y. Xia, *Energy Environ. Sci.*, 2012, **5**, 6652.
- X. Zhang, P. S. Kumar, V. Aravindan, H. H. Liu, J. Sundaramurthy, S. G. Mhaisalkar, H. M. Duong, S. Ramakrishna and S. Madhavi, *J. Phys. Chem. C*, 2012, **116**, 14780.
- S. H. Nam, H. S. Shim, Y. S. Kim, M. A. Dar, J. G. Kim and W. B. Kim, *Appl. Mater. Interface*, 2010, **2**, 2046.
- Y. S. Hu, L. Kienle, Y. G. Guo and J. Maier, *Adv. Mater.*, 2006, **18**, 1421.
- A. S. Arico, P. Bruce, B. Scrosati, J. M. Tarascon and W. V. Schalkwijk, *Nat. Mater.*, 2005, **4**, 366.
- H. Liu, L. J. Fu, H. P. Zhang, J. Gao, C. Li, Y. P. Wu and H. Q. Wu, *Electrochem. Solid-State Lett.*, 2006, **9**, A529.
- S. Liu, G. L. Pan, N. F. Yan and X. P. Gao, *Energy Environ. Sci.*, 2010, **3**, 1732.
- C. L. Olson, J. Nelson and M. S. Islam, *J. Phys.Chem.C*, 2006, **110**, 9995.
- S. W. Kim, T. H. Han, J. Kim, H. Gwon, H. S. Moon, S.W. Kang, S. O. Kim and K. Kang, *ACS Nano*, 2009, **3**, 1085.
- F. X. Wu, Z. X. Wang, X. H. Li and H. J. Guo, *J. Mater. Chem.*, 2011, **21**, 12675.
- J. M. Li, W. Wan, H. H. Zhou, J. J. Li and D. S. Xu, *Chem. Commun.*, 2011, **47**, 3439.
- Y. M. Chen, Q.R. Qian, X. P. Liu, L. R. Xiao and Q. H. Chen, *Mater. Lett.*, 2010, **64**, 6.
- S. Selvam, M. Sundrarajan, *Polymer*, 2012, **87**, 1419.
- H. Wu, G. Chan, J. W. Choi, I. Ryu, Y. Yao, M. T. Mcdowell, S. W. Lee, A. Jackson, Y. Yang, L.B. Hu and Y. Cui, *Nat. Nanotechnol.*, 2012, **7**, 310.

19. B. Erdem, R. A. Hunsicker, G. W. Simmons, E. D. Sudol, V. L. Dimonie and M. S. El-Aasser, *Langmuir*, 2001, **17**, 2664.
20. L. Zhang, G. Q. Shi, *J. Phys. Chem. C*, 2011, **115**, 17206.
21. T. Xu, W. Hou, X. Shen, H. Wu, X. Li, J. Wang and Z. Jiang, *J. Power Sources*, 2011, **196**, 4934.
22. R. R. Schlittler, J. W. Seo, J. K. Gimzewski, C. Durkan, M. S. M. Saifullah and M. E. Welland, *Science*, 2001, **292**, 1136.
23. W. Zhang, B. S. Zhang and T. L. Shao, *J. Phys. Chem. C*, 2011, **115**, 20550.
24. R. D. Leapman, L. A. Grunes and P. L. Fejes, *Phys. Rev. B*, 1982, **26**, 614.
25. M. He, Z. H. Zhang, *J. Phys. Chem. C*, 2010, **114**, 13068.
26. F. Pailloux, D. Imhoff, T. Sikora, A. Barthélémy, J. L. Maurice, J. P. Contour, C. Colliex and A. Fert, *Phys. Rev. B*, 2002, **66**, 014417.
27. L. S. Zhong, J. S. Hu, L. J. Wan and W. G. Song, *Chem. Commun.*, 2008, **10**, 1184.
28. Y. G. Guo, Y. S. Hu and J. Maier, *Chem. Commun*, 2006, **26**, 2783.
29. Y. M. Chen, Z. G. Lu, L. M. Zhou, Y. W. Mai and H. T. Huang, *Nanoscale*, 2012, **4**, 6800.
30. Z. J. Fan, J. Yan, T. Wei, G. Q. Ning, L. J. Zhi, J. C. Liu, D. X. Cao, G. L. Wang and F. Wei, *ACS Nano*, 2011, **5**, 2787.
31. D. Deng, M. G. Kim, J. Y. Lee and J. Cho, *Energy Environ. Sci.*, 2009, **2**, 818.
32. J. R. Li, Z. L. Tang and Z. T. Zhang, *Electrochem. Solid-state Lett.*, 2005, **8**, A316.
33. Y. K. Choi, K. I. Chung, W. S. Kim and Y. E. Sung, *Microchem. J.*, 2001, **68**, 61.
34. M. Hibino, K. Abe, M. Mochizuki and M. Miyayama, *J. Power Sources*, 2004, **126**, 139.
35. M. D. Wei, Z. M. Qi, M. Ichihara, I. Honma and H. S. Zhou, *Chem. Phys. Lett.*, 2006, **424**, 316.
36. C. H. Jiang, I. Honma, T. Kudo and H. S. Zhou, *Electrochem. Solid-State Lett.*, 2007, **10**, A127.
37. B. Zhang, Y. Yu, Z. D. Huang, Y. B. He, D. Jang, W. S. Yoon, Y. W. Mai, F. Y. Kang and J. K. Kim, *Energy Environ. Sci.*, 2012, **5**, 9895.
38. L. F. Shen, C. Z. Yuan, H. J. Luo, X. G. Zhang, K. Xu and F. Zhang, *J. Mater. Chem.*, 2011, **21**, 761.
39. L. F. Shen, X. G. Zhang, H. S. Li, C. Z. Yuan and G. Z. Cao, *J. Phys. Chem. Lett.*, 2011, **2**, 3096.
40. J. X. Qiu, P. Zhang, M. Ling, S. Li, P. Liu, H. J. Zhao and S. Q. Zhang, *ACS Appl. Mater. Interfaces*, 2012, **4**, 3636.
41. C. Q. Feng, J. Tang, C. F. Zhang and R. Zeng, *Nanosci. Nanotechnol. Lett.*, 2012, **4**, 430.
42. H. Huang, J. W. Fang, Y. Xia, X. Y. Tao, Y. P. Gan, J. Du, W. J. Zhu and W. K. Zhang, *J. Mater. Chem. A*, 2013, **1**, 2495.
43. Y. G. Guo, F. F. Cao, S. F. Zheng, X. L. Wu, L. Y. Jiang, R. R. Bi, L. J. Wan and J. Maier, *Chem. Mater.*, 2010, **22**, 1908.
44. H. W. Bai, Z. Y. Liu and D. D. Sun, *J. Mater. Chem.*, 2012, **22**, 24552-24557.
45. Y. M. Chen, X. Y. Li, K. Park, J. Song, J. H. Hong, L. M. Zhou, Y. W. Mai, H. T. Huang and J. B. Goodenough, *J. Am. Chem. Soc.*, 2013, **135**, 16280.

**A table of contents entry**

Porous TiO<sub>2</sub>-carbon nanofiber anode shows high capacity of ~680 mA h g<sup>-1</sup> after 250 cycles at 0.1 A g<sup>-1</sup>.

